Int. J. Heat Mass Transfer. Vol. 29, No. 11, pp. 1617–1628, 1986
Printed in Great Britain

0017-9310/86 $3.00 + 0.00
Pergamon Journals Ltd.

Effect of interbaffle spacing on heat transfer and pressure drop in a shell-and-tube heat exchanger

E. M. SPARROW and L. G. REIFSCHNEIDER
Department of Mechanical Engineering, University of Minnesota, Minneapolis, MN 55455, U.S.A.

(*Received* 16 *December* 1985 *and in final form* 3 *March* 1986)

Abstract—Experiments have been performed to determine the response of the heat (mass) transfer and pressure drop on the shell side of a shell-and-tube heat exchanger to changes in the interbaffle spacing. Per-tube, per-row and per-compartment heat (mass) transfer coefficients were obtained by means of the naphthalene sublimation technique, all for the fully developed regime. Pressure distribution measurements were made throughout the heat exchanger, and the pattern of fluid flow was visualized with the aid of the oil–lampblack technique. The greatest sensitivity of the per-tube heat transfer coefficient to the interbaffle spacing occurred at the tubes situated in the inflow window of a compartment, where higher coefficients (by about 15%) were encountered for larger interbaffle spacings. In the crossflow zone, the per-tube transfer coefficients corresponding to the smaller interbaffle spacing exceeded those for the larger interbaffle spacing by about 5%, and similarly in the baffle-adjacent row in the outflow window of the compartment. The other rows in the outflow window were ambivalent about the effects of interbaffle spacing. Owing to cancellations among the aforementioned per-tube responses, the compartment-average transfer coefficients were virtually unaffected by the spacing. The per-compartment pressure drop decreased as the interbaffle spacing decreased, but for a fixed streamwise length, the pressure drop was slightly larger for smaller spacings. The experimental results were compared with the predictions of the Tinker and Delaware Project design methods.

INTRODUCTION

THIS paper describes the concluding phase of a two-part, fundamental-level investigation of shell side heat transfer and pressure drop in a shell-and-tube heat exchanger. In the first part [1], primary attention was focused on the response of the heat transfer and pressure drop to the size of the windows in the segmental baffles of the heat exchanger. Here, the effect of the spacing between successive baffles is investigated. In both parts of the work, the Reynolds number was varied parametrically.

The research to be described here may be elaborated by reference to Fig. 1. Part (a) of the figure shows a longitudinal cross section of the heat exchanger used in the present experiments, while part (b) is a similar view of the heat exchanger of [1]. The tubes have been omitted to preserve clarity. As seen from the figure, the interbaffle spacing used here is about 2/3 of that of ref. [1]. It can be conjectured that a change in the interbaffle spacing will affect both the way in which the flow executes the 180° turns and the extent to which true crossflow is achieved relative to the tubes in any compartment. It would be expected that such spacing-related alterations of the fluid flow would affect both the heat transfer and pressure drop characteristics.

The experiments were performed by employing naphthalene sublimation, a mass transfer technique, with the tubes of the heat exchanger being modeled by naphthalene-coated rods and with air as the shell side fluid. The use of the naphthalene technique obviated the need for a tubeside fluid. Conversion of the mass transfer results to heat transfer results was

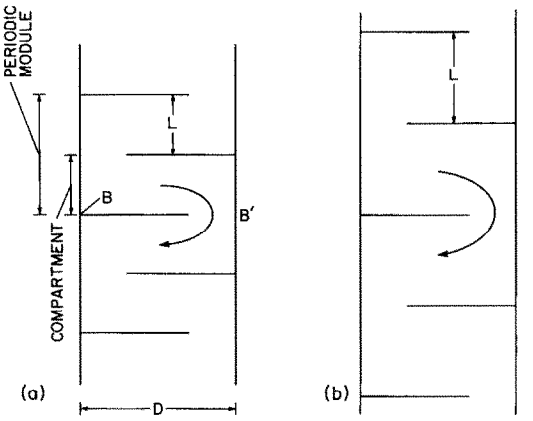

FIG. 1. Longitudinal cross sections illustrating the investigated interbaffle spacings (the tubes have been omitted to preserve clarity).

accomplished by employing the analogy between the two transport processes.

Mass transfer coefficients were determined at each tube in a typical compartment of the heat exchanger [illustrated in Fig. 1(a)] situated in the hydrodynamically developed regime. The per-tube values were used to obtain both row-average and compartment-average results. Averages were also taken over two consecutive compartments to obtain per-tube results which are truly representative of the fully developed regime.

Per-compartment pressure drops as well as the pressure drops within a compartment were measured by means of an array of pressure taps situated internal

NOMENCLATURE

A_{min}	minimum free-flow area, equation (7)
D	inside diameter of shell
d	tube diameter
$\mathscr{D}$	mass diffusion coefficient
H	baffle window opening
i	row number
j	transverse position of tube
K_m	per-tube mass transfer coefficient
K_p	per-compartment pressure loss coefficient
L	interbaffle spacing
p	local pressure in heat exchanger
p_∞	ambient pressure
Δp	per-compartment pressure drop
Re	Reynolds number, $\rho V^* d/\mu$
Sc	Schmidt number
Sh	per-tube Sherwood number in a compartment
Sh_{comp}	compartment-average Sherwood number
Sh_{mod}	average Sherwood number for two-compartment module
Sh_{row}	row-average Sherwood number in a compartment
$Sh_{tube/mod}$	per-tube Sherwood number in a two-compartment module
S_L	longitudinal pitch
S_T	transverse pitch
t	baffle thickness
V^*	mean velocity in minimum free-flow area
$\dot{w}$	mass flow rate.

Greek symbols

μ	viscosity
ν	kinematic viscosity
ρ	density.

to the heat exchanger. Flow visualization was performed via the oil–lampblack technique, and a representative visualization pattern will be presented.

The effect of interbaffle spacing will be established by comparisons of the present heat/mass transfer and pressure drop results with those of ref. [1]. In addition, the design methods of Tinker [2, 3] and of the Delaware Project [4, 5] will be evaluated with regard to the effect of interbaffle spacing on the heat/mass transfer and pressure drop.

EXPERIMENTS

The heat exchanger used here is a completely rebuilt version of that of ref. [1]. In the rebuilding process, all dimensions were strictly preserved aside from the interbaffle spacing. Therefore, the detailed description of the apparatus set forth in ref. [1] continues to apply, so that only a broad overview need be given here. The heat exchanger was designed and built to be totally free of leakage paths and to have negligible bypass effects according to the criterion of ref. [4].

Figure 2 is a cross-sectional view of the heat exchanger. The cross section may be oriented with respect to the longitudinal section by matching the letters B and B′ in Figs. 2 and 1(a). All told, there are 92 tubes in the cross section deployed in an equilateral triangular pattern with a transverse pitch S_T and a longitudinal pitch S_L. Only 49 tube positions are unique—those shown in Fig. 2. The space below the symmetry line BB′ is filled with tubes positioned at mirror-image locations with respect to those shown.

There are 11 rows of tubes in each cross section. The individual tubes are identified by a two-address system, as illustrated in Fig. 2. The first number in the address designates the row (increasing row numbers in the flow direction), while the second number indicates the transverse position of the tube in the row, with the numeral one being assigned to the tube nearest the symmetry line BB′. For the selected baffle window opening, rows 1–3 are situated in the inflow window of the compartment, and rows 9–11 are in the outflow window. The intermediate rows, 4–8, are situated in the so-called crossflow zone, which is the portion of the compartment between the inflow and outflow windows.

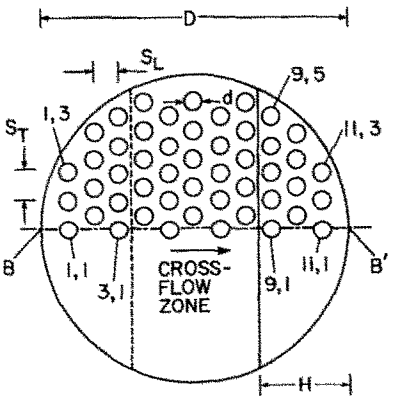

FIG. 2. Cross-sectional view of the heat exchanger.

The dimensions defining the heat exchanger include the tube diameter d, the transverse and longitudinal pitches S_T and S_L, the interbaffle spacing L, the inside diameter D of the shell, the baffle window opening H, and the baffle thickness t. With respect to the objectives of the research reported here, all dimensions aside from L may be regarded as constant with respective (nondimensionalized) values

$$d/D = 0.061, \quad S_T/d = 1.5, \quad S_L/d = 1.3,$$
$$H/D = 0.302, \quad t/D = 0.015. \quad (1)$$

The interbaffle spacing L is measured between the facing surfaces of consecutive baffles. The L/D value for the heat exchanger used in the present experiments

was 0.385, while that of ref. [1] was 0.585. In terms of actual dimensions, it is sufficient to note that $D = 10.41$ cm (4.10 in.) and to compute the other quantities from the aforementioned ratios.

The heat exchanger was synthesized from a stack of seven compartments, with the mass transfer test section situated in the fourth and fifth compartments. The mass transfer coefficients were determined from the change of mass of naphthalene-coated tubes during the course of a data run. To facilitate the removal of the coated tubes for weighing both before and after the data run, the test section was designed so that access to its interior could be gained within seconds. This was accomplished by lifting the upper portion of the heat exchanger away from the lower portion. The weighing of the naphthalene-coated tubes was performed with an electronic analytical balance having a resolution of 10^{-5} g.

All of the tubes in the mass transfer test section were made removable. During any given data run, only one naphthalene-coated tube was utilized, while the other tubes were metallic. In a sequence of runs, the location of the naphthalene-coated tube was varied systematically in order to obtain data at all 49 unique tube positions in the cross section.

The diameters of all the tubes, naphthalene-coated and metallic, were identical. The naphthalene coating was applied by dipping a cylindrical metallic substrate into a bath of molten naphthalene, followed by machining on a lathe to achieve the desired diameter.

Thermocouples were installed to measure the temperature in the test section and to verify its constancy during the course of a data run. Since the vapor pressure of naphthalene is a strong function of temperature, the constancy of the temperature is a prerequisite for the attainment of a timewise constant rate of sublimation from a naphthalene-coated tube to the air stream. Temperature constancy was achieved by allowing an equilibration period prior to the initiation of each data run.

For the pressure drop measurements, a total of 17 taps were installed in the heat exchanger. Three taps were installed in the shell wall in each compartment. One of the three taps was at the inflow end of the compartment, the second was at the middle of the crossflow zone, and the third was at the outflow end (an inflow-end tap could not be provided in the first compartment, and the last compartment was uninstrumented). The pressure measurements were made in a series of runs separate from the mass transfer runs. The pressure signals were detected by a solid-state pressure meter having a resolution of 10^{-3} Torr.

The apparatus was operated in the open-circuit mode and in suction, with air from the naphthalene-free, temperature-controlled laboratory drawn into an opening in the shell wall of the first compartment. After traversing the heat exchanger, the air passed through a flow meter (a calibrated orifice) and a control valve, and then was ducted to a blower. The blower was situated in a service corridor adjacent to the laboratory, and its compression-heated, naphthalene-enriched discharge was vented outside the building.

The oil–lampblack technique [6] was used for the flow visualization. This technique provides an indication of the flow pattern adjacent to a surface in terms of the response of an oil–lampblack mixture, previously applied to the surface, to the forces exerted by the flowing fluid. In regions of high and intermediate velocity, the mixture moves over the surface under the action of the shear forces, leaving an array of streaks which indicate the direction of the fluid flow. In regions of low velocity, the shear stresses are small and the fluid remains stationary.

To obtain a definitive visualization pattern, the fluidity of the oil–lampblack mixture had to be tailored both to accommodate the magnitude of the shear stresses exerted by the flowing fluid and the possibility of sag due to gravity. In order to have a permanent record of the visualization pattern, the surfaces of the heat exchanger were covered with white, plasticized, self-adhering contact paper before application of the mixture. The contact paper was removed from the surfaces at the end of each visualization run and photographed.

DATA REDUCTION

The first quantity to be evaluated is the mass transfer coefficient K_m at each tube in the cross section. If ΔM is the sublimation-related change of mass at a tube during the duration τ of a data run, and A is the transfer surface area of the tube, then

$$K_m = (\Delta M/\tau)/A(\rho_{nw} - \rho_{nb}) \tag{2}$$

where ρ_{nw} and ρ_{nb} are, respectively, the densities of naphthalene vapor at the subliming surface and in the bulk flow. The former was evaluated from the vapor pressure–temperature relation corresponding to solid–vapor equilibrium [7] in conjunction with the perfect gas law, using the measured test section temperature as input. For the present experiments, $\rho_{nb} = 0$.

In dimensionless form, the per-tube mass transfer coefficients will be reported in terms of the Sherwood number

$$Sh = K_m d/\mathscr{D}. \tag{3}$$

The naphthalene–air diffusion coefficient $\mathscr{D}$ which appears in equation (3) can be eliminated by employing the definition of the Schmidt number ($Sc = \nu/\mathscr{D}$), so that $Sh = (K_m d/\nu)Sc$, and ν is the kinematic viscosity of air. For naphthalene diffusion in air, $Sc = 2.5$ [7].

It was pointed out in ref. [1] that a given tube does not have the same value of the heat (or mass) transfer coefficient in consecutive compartments, even in the fully developed regime. This is because the pattern of fluid flow reverses from compartment to compartment. As a consequence of these reversals, an identical fluid flow field recurs in *every other* compartment and, correspondingly, the per-tube mass transfer coefficient

for a given tube takes on the same value in every other compartment. In fact, there are two such recurring values for each tube, one for each of the consecutive compartments.

Rather than having to specify the two recurring values for each tube, it is more appropriate to specify a single value which would serve as the fully developed per-tube transfer coefficient. To this end, a module consisting of two consecutive compartments is considered. For any given tube, the values of the per-tube transfer coefficients in the two compartments are averaged. The per-tube Sherwood numbers resulting from the averaging are denoted as $Sh_{\text{tube/mod}}$.

The averaging to determine $Sh_{\text{tube/mod}}$ is straightfoward. For example, a tube at position 2,3 in one compartment is at position 10,3 in the next compartment. So, for that tube,

$$Sh_{\text{tube/mod}} = [Sh(2,3) + Sh(10,3)]/2. \tag{4}$$

The per-tube Sherwood numbers can also be utilized to evaluate the average Sherwood number Sh_{row} for each row in a compartment. For the averaging, it is convenient to let the index i denote the row number ($i = 1$ to 11) and the index j denote the transverse positions of individual tubes in a row ($j = 1$ to J where, according to Fig. 2, $J = 3$, 4 or 5). Then, for any row,

$$Sh_{\text{row}} = \left[\sum_{j=1}^{J} Sh(i,j)\right] \Big/ J. \tag{5}$$

In addition, the averaging can be extended over all 92 tubes in a compartment to yield Sh_{comp}. Since the value of Sh_{comp} is the same for all compartments in the fully developed regime, it follows that the average Sherwood number Sh_{mod} for a two-compartment module is equal to Sh_{comp}. Then,

$$Sh_{\text{comp}} = Sh_{\text{mod}} = \left[\sum_{i,j} Sh(i,j)\right] \Big/ 92. \tag{6}$$

As noted earlier, the Sherwood number results can be transformed to Nusselt numbers by employing the analogy between heat and mass transfer. The transformation is discussed in ref. [1] and need not be repeated here.

Attention will now be turned to the data reduction for the pressure drop. As was mentioned in the preceding section, each compartment was equipped with three pressure taps, enabling three independent determinations of the per-compartment pressure drop Δp. As will be demonstrated later, the three values of Δp were virtually identical, and the small differences among them were averaged out.

For a dimensionless presentation of the pressure drop results, it is necessary to define a characteristic velocity. Here, the mean velocity at the minimum free-flow area in the row of tubes situated in the widest part of the cross section will be used (i.e. row 6). At that row, there are 10 tubes, so that

$$A_{\min} = (D - 10d)L \tag{7}$$

and

$$V^* = \dot{w}/\rho A_{\min} \tag{8}$$

in which $\dot{w}$ is the rate of mass flow in the heat exchanger, and ρ is the mean air density in the fully developed region. Then, a per-compartment pressure loss coefficient K_p was evaluated as

$$K_p = \Delta p / \tfrac{1}{2}\rho V^{*2}. \tag{9}$$

The mass (heat) transfer and pressure drop results will be parameterized by the Reynolds number

$$Re = \rho V^* d/\mu \tag{10}$$

from which ρV^* can be eliminated with the aid of equation (8), yielding

$$Re = \dot{w} d/\mu A_{\min}. \tag{11}$$

RESULTS AND DISCUSSION

Per-tube Sherwood numbers

The Sherwood numbers at each of the unique tube positions in a compartment are presented in Figs. 3–5. Each figure is a composite consisting of several graphs, with each graph serving to convey results for a given row. In particular, the graphs of Fig. 3 convey results for rows 1–4, those of Fig. 4 for rows 5–8, and those of Fig. 5 for rows 9–11.

The main focus of Figs. 3–5 is to compare the per-tube Sherwood numbers for the present interbaffle spacing ($L/D = 0.385$) with those for the interbaffle spacing of ref. [1] ($L/D = 0.585$). To enable such comparisons to be made with complete clarity, it is necessary to avoid overlap of data corresponding to the various transverse tube positions in a given row (i.e. the j positions). To separate the data for the various transverse positions, the scheme set forth in the legend of Fig. 5 has been adopted. As indicated there, the Sherwood number at the transverse position $j = 1$ has been plotted as such, while the Sherwood numbers at positions $j = 2, 3, \ldots$ have been plotted as $1.2Sh$, $(1.2)^2 Sh, \ldots$, respectively. Thus, for example, for row 1 (Fig. 3, upper left), the $j = 1$ data lie lowest in the graph, above which are the $j = 2$ data and the $j = 3$ data, in that order.

In each graph, the Sherwood number (or its scaled version) is plotted as a function of the Reynolds number. The open data symbols represent the results for the $L/D = 0.385$ interbaffle spacing (present case), while the black symbols depict the data for $L/D = 0.585$ [1]. The $L/D = 0.385$ data at each tube position have been interconnected by a least-squares straight line, which corresponds to the power-law relation $Sh = CRe^n$.

Attention may first be focused on rows 1–3, which are situated in the inflow window of the compartment. It is seen that in both rows 1 and 2, the Sherwood numbers for the $L/D = 0.585$ spacing clearly exceed

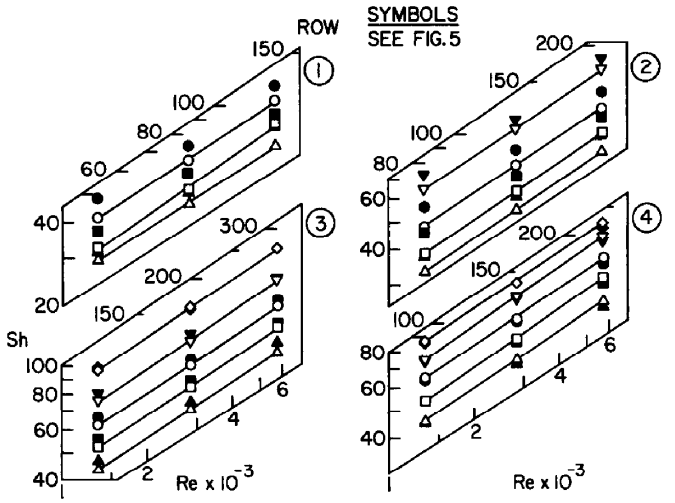

FIG. 3. Per-tube Sherwood numbers at tubes situated in rows 1–4 in a compartment for $L/D = 0.385$ (open symbols) and 0.585 (black symbols).

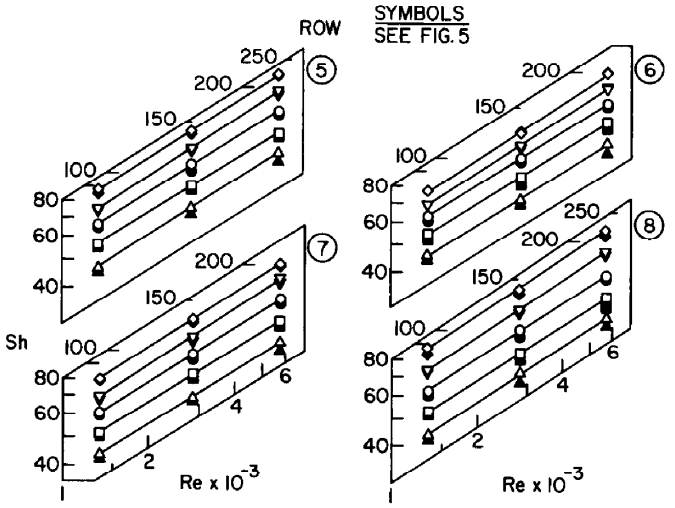

FIG. 4. Per-tube Sherwood numbers at tubes situated in rows 5–8 in a compartment for $L/D = 0.385$ (open symbols) and 0.585 (black symbols).

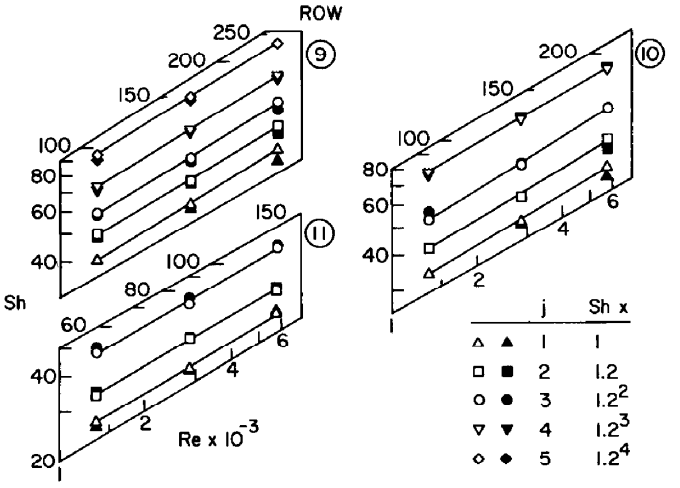

FIG. 5. Per-tube Sherwood numbers at tubes situated in rows 9–11 in a compartment for $L/D = 0.385$ (open symbols) and 0.585 (black symbols).

those for the $L/D = 0.385$ spacing, with the deviations being as large as 15%. The same qualitative relationship prevails in the third row, but the quantitative deviations are considerably smaller.

In the crossflow zone, rows 4–8, the opposite relationship applies, that is, the Sherwood numbers for the $L/D = 0.385$ spacing generally exceed those for the $L/D = 0.585$ spacing. The deviations are, for the most part, in the 5% range. It also appears that the Sherwood number is slightly more sensitive to L/D at positions nearer the symmetry line than at positions nearer the shell wall.

Rows 9–11 are in the outflow window of the compartment. The results for row 9 are similar to those for the crossflow zone with regard to the L/D effect. However, in rows 10 and 11, the results are ambivalent with respect to L/D. There is a tendency for the $L/D = 0.385$ results to slightly exceed those for $L/D = 0.585$ at positions nearer the symmetry line, with a reverse relationship at positions nearer the shell wall.

To rationalize these findings, it may be observed that a smaller interbaffle spacing produces a more channeled flow in the crossflow zone. In turn, this channeling alters the path followed by the fluid as it turns through the baffle window from the outflow end of one compartment into the inflow end of the next compartment. In particular, the turning occurs farther from the baffle edge and is sharper.

The more channeled nature of the flow is responsible for the observed higher Sherwood numbers in the crossflow zone and in the adjacent row in the outflow window (i.e. in row 9). On the other hand, the turning flow washes the back sides of the tubes in the inflow window to a lesser extent, which reduces the Sherwood numbers at those tubes.

The results presented in Figs. 3–5 conveyed the per-tube Sherwood numbers at all tubes situated within a given compartment. Attention is now turned to the per-tube Sherwood numbers $Sh_{\text{tube/mod}}$ for a two-compartment module. This information is given in Table 1 where, to provide greater generality, the ratio of $Sh_{\text{tube/mod}}$ to the module-average Sherwood number Sh_{mod} (averaged over all tubes) is listed. The table is subdivided into (a), (b) and (c) parts, respectively for Reynolds numbers of 1350, 2850 and 5750.

Owing to the two-compartment averaging, the $Sh_{\text{tube/mod}}$ values at corresponding tubes in rows 1 and 11 are identical, and similarly for rows 2 and 10, 3 and 9, etc. This commonality is indicated in the row listing in Table 1 (left-hand column). A horizontal line has been drawn in the table to separate the window rows (1–3 and 9–11) from the crossflow rows (4–8). As before, the index j designates the transverse position of a tube in a row. Note that for each tube position, there are two entries. The first entry corresponds to $L/D = 0.385$, while the second entry is for $L/D = 0.585$. As will be documented later, Sh_{mod} is virtually the same for $L/D = 0.385$ and 0.585 at each Reynolds number, so that a comparison of $Sh_{\text{tube/mod}}/Sh_{\text{mod}}$ values for the two L/D is tantamount to comparing $Sh_{\text{tube/mod}}$ values.

Table 1. Values of $Sh_{\text{tube/mod}}/Sh_{\text{mod}}$ for $L/D = 0.385$ (first entry) and $L/D = 0.585$ (second entry)

(a) $Re = 1350$

Row	j = 1	2	3	4	5
1,11	0.70	0.69	0.77		
	0.71	0.74	0.84		
2,10	0.84	0.84	0.87	1.02	
	0.89	0.89	0.97	1.05	
3,9	1.04	1.06	1.05	1.07	1.14
	1.08	1.07	1.06	1.08	1.13
4,8	1.10	1.09	1.09	1.06	1.03
	1.07	1.07	1.05	1.04	1.00
5,7	1.12	1.11	1.09	1.03	1.00
	1.08	1.07	1.06	1.00	0.97
6	1.13	1.12	1.08	0.98	0.91
	1.08	1.06	1.02	0.97	0.90

(b) $Re = 2850$

j = 1	2	3	4	5
1,11	0.69	0.68	0.74		
	0.72	0.73	0.80		
2,10	0.83	0.82	0.86	1.01	
	0.86	0.88	0.94	1.04	
3,9	1.05	1.04	1.04	1.07	1.16
	1.06	1.07	1.06	1.09	1.14
4,8	1.12	1.10	1.09	1.08	1.03
	1.07	1.06	1.05	1.06	1.02
5,7	1.13	1.12	1.10	1.05	1.01
	1.08	1.07	1.05	1.02	0.99
6	1.11	1.11	1.08	0.99	0.92
	1.07	1.05	1.04	0.99	0.93

(c) $Re = 5750$

j = 1	2	3	4	5
1,11	0.69	0.69	0.75		
	0.76	0.73	0.81		
2,10	0.83	0.82	0.86	0.98	
	0.86	0.86	0.93	1.04	
3,9	1.04	1.05	1.05	1.08	1.16
	1.06	1.05	1.05	1.09	1.18
4,8	1.11	1.11	1.09	1.09	1.05
	1.07	1.06	1.06	1.06	1.01
5,7	1.11	1.10	1.09	1.07	1.00
	1.04	1.06	1.05	1.04	1.00
6	1.11	1.10	1.01	1.00	0.93
	1.04	1.04	1.05	1.02	0.96

As can be seen in the table, the lowest values of $Sh_{\text{tube/mod}}$ are in rows 1 and 11, i.e. in the most-outboard rows of the inflow and outflow windows. Here, Sherwood numbers that are 30% below the module average value are in evidence. Higher Sherwood numbers occur in the intermediate window rows (2 and 10), with still higher values in the baffle-adjacent win-

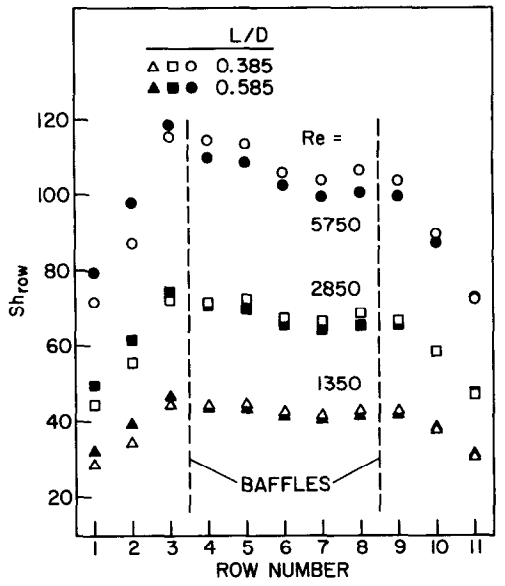

FIG. 6. Row-average Sherwood numbers in a compartment for $L/D = 0.385$ and 0.585.

dow rows (3 and 9). Note that in all the window rows, there is a tendency for the Sherwood number to increase in the direction of increasing j (i.e. from the symmetry line to the shell wall). In fact, the highest Sherwood number in the heat exchanger occurs at $j = 5$ for rows 3 and 9—about 15% above the compartment average value.

In the crossflow zone, there are only slight row-to-row differences. In contrast to the aforementioned trend in the window zones, the Sherwood numbers in the crossflow zone decrease in the direction from the symmetry line to the shell wall (i.e. with increasing j). For the most part, the values of $Sh_{\text{tube/mod}}/Sh_{\text{mod}}$ in the crossflow zone exceed unity.

The qualitative relationships between the tabulated results for the two interbaffle spacings are as set forth in the discussion of Figs. 3–5, but the extent of the deviations is moderated by the two-compartment averaging.

Row, compartment and module Sherwood numbers

The Sherwood numbers Sh_{row} for each row in a compartment are plotted in Fig. 6 as a function of the row number. The data are parameterized by the Reynolds number and by the interbaffle spacing. Module-based values of the row Sherwood number are readily determined by averaging the appropriate compartment-based values of Fig. 6. For example, the module-based Sherwood number for either of rows 3 or 9 is obtained by averaging the plotted Sh_{row} values for rows 3 and 9.

As seen in Fig. 6, the row-by-row variation of the Sherwood number has the same form for the two investigated interbaffle spacings. Starting with a relatively low value in the first row, the Sherwood number increases substantially in the succeeding rows of the inflow window, attaining a maximum just upstream of the baffle edge. In the crossflow zone, the row-by-row variations are moderate, but there is an overall downward trend. In the outflow window, the Sherwood number decreases from row to row, with the extent of the decrease being comparable to the increase which occurs in the inflow window.

Table 2. Values of $Sh_{\text{comp}} = Sh_{\text{mod}}$

	L/D	
Re	0.385	0.585
1350	40.48	40.71
2850	64.56	64.32
5750	101.38	100.19

The greatest effects of interbaffle spacing are in evidence in the inflow window, where larger Sherwood numbers correspond to the larger spacing. The Sherwood numbers in the crossflow zone are less sensitive to the interbaffle spacing, but those for the smaller spacing are consistently higher. Even lesser sensitivity is in evidence in the outflow window, and there is some inconsistency as to whether the $L/D = 0.385$ results or the $L/D = 0.585$ results lie higher.

The compartment-average and module-average Sherwood numbers, Sh_{comp} and Sh_{mod}, are listed in Table 2. The tabulated results show that, despite spacing-related differences in the per-tube Sherwood numbers and the row Sherwood numbers, the compartment and module Sherwood numbers were virtually unaffected by the interbaffle spacing. In particular, the maximum spacing-related deviation in evidence in Table 2 is about 1.2%. The local per-tube deviations have, therefore, canceled out in the averaging process. Thus, if only the overall heat or mass transfer characteristics are of interest, changes in the interbaffle spacing in the investigated range are not an issue.

Pressure drop results

The distribution of pressure throughout the heat exchanger is presented in Fig. 7 for a representative case. Also included in the figure, at the upper left, is a diagram showing the layout of the pressure taps. As seen there, taps 1–6 are situated at the center of the crossflow zone in the successive compartments, taps 7–12 are at the outflow ends of the compartments, and taps 13–17 are at the inflow ends of the compartments. In the fully developed regime, the pressure drops between successive inflow-end taps, between successive outflow-end taps, and between successive center taps should be the same.

The pressure is plotted on the ordinate in dimensionless terms, where p_∞ is the pressure in the ambient from which the air was drawn, p is the pressure at a tap location, and $\frac{1}{2}\rho V^{*2}$ is the characteristic dynamic pressure. As seen in the figure, the pressures naturally fall along three straight lines, respectively for the inflow-end taps, the center taps, and the outflow-end

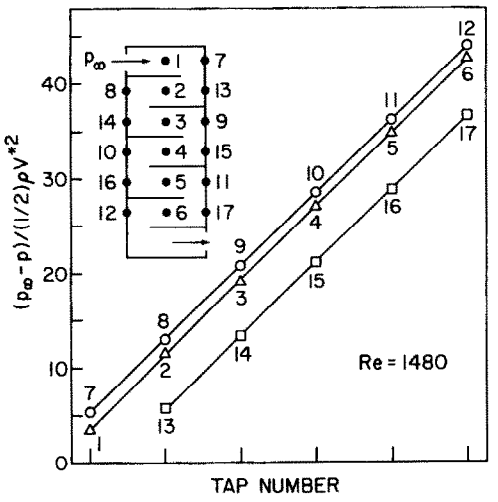

FIG. 7. Representative pressure distribution throughout the heat exchanger ($L/D = 0.385$, $Re = 1480$).

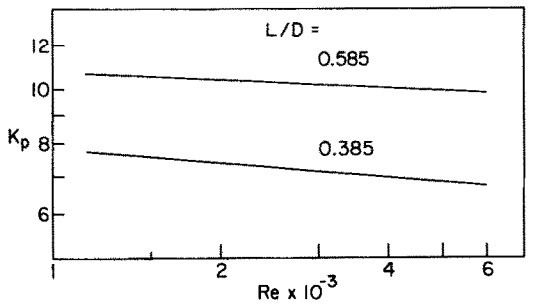

FIG. 8. Per-compartment pressure loss coefficients for $L/D = 0.385$ and 0.585.

taps. The lines, determined via least-squares, are virtually parallel. Their slopes, when averaged, yielded the pressure drop Δp per compartment which was used as input for the evaluation of the pressure loss coefficient K_p.

Further inspection of Fig. 7 shows that the pressure drop between the inflow end and the center of a compartment is substantially greater than the pressure drop between the center and the outflow end, which is consistent with the nature of the flow pattern. Also noteworthy is the fact that the pressure data for all compartments, including the first compartment, fall squarely on the straight lines, thereby indicating the very rapid hydrodynamic development of the flow.

The per-compartment pressure loss coefficients for both the $L/D = 0.385$ and 0.585 interbaffle spacings are plotted in Fig. 8 as a function of the Reynolds number, with the respective representations

$$K_p = 14.02Re^{-0.0838}, \quad K_p = 15.95Re^{-0.0555}. \quad (12)$$

Note that for both cases, there is a weak dependence of K_p on the Reynolds number, as befits flows in which inertial losses play a dominant role relative to skin friction. The slightly greater dependence for the case of the smaller spacing may reflect the greater role of the baffle surfaces and the more compact turning of the flow.

Table 3. Comparison of predicted Sh_{comp} and K_p values for $L/D = 0.385$ and $L/D = 0.585$

	$Sh(0.585)/Sh(0.385)$			$K_p(0.585)/K_p(0.385)$		
Re	T	D	Exp	T	D	Exp
1350	1.06	1.01	1.01	1.19	1.30	1.39
2850	1.06	1.01	1.00	1.19	1.31	1.42
5750	1.06	1.01	0.99	1.19	1.33	1.46

Figure 8 indicates that the per-compartment pressure loss for the $L/D = 0.385$ baffle spacing is, on the average, about 70% of that for the $L/D = 0.585$ baffle spacing. However, 1.52 of the former compartments are needed to provide the same heat transfer surface (of the tubes) as is provided by one compartment of the latter. Thus, for the same heat transfer surface area, the pressure drop for the $L/D = 0.385$ baffle spacing is about 6% greater than that for the $L/D = 0.585$ spacing. Therefore, from the pressure drop standpoint, the latter is very moderately advantageous.

Comparisons with design methods

Design methods are available for the prediction of the compartment Sherwood number and K_p values. The methods to be employed here are those of Tinker [2, 3] and of the Delaware Project [4, 5]. The application of these methods to the heat exchanger of ref. [1] has been set forth in detail in ref. [8], and the present application differs only in that a different numerical value of the interbaffle spacing L is used. Therefore, the evaluation of the design methods will be omitted here, and only the final results will be presented.

There are, however, a few comments which are relevant with regard to the application of the Delaware Project method. In ref. [8], it was found that the treatment of the bypass effect as specified in the original version of the method [4] gave better agreement with the experimental results of ref. [1] than did the treatment specified in the updated version [5]. Consequently, the original treatment of the bypass effect will be used here. Also, the application of the method requires that heat transfer coefficients for crossflow tube banks be provided as input. In ref. [8], crossflow heat transfer coefficients from various literature sources were employed, and those of the Whitaker correlation [9] yielded results that agreed best with the experimental data. The Whitaker correlation will, therefore, be used here in implementing the Delaware method.

Table 3 lists the ratios $Sh(0.585)/Sh(0.385)$ and $K_p(0.585)/K_p(0.385)$ predicted by the Tinker method (T) and the Delaware Project method (D), where $Sh(0.585)$ and $Sh(0.385)$ respectively denote the compartment Sherwood numbers for $L/D = 0.585$ and 0.385, and similarly for $K_p(0.585)$ and $K_p(0.385)$. The Sherwood numbers correspond to $Sc = 2.5$. Also included in the table for comparison purposes are the values of the ratios obtained by using the present data in conjunction with that of ref. [1].

Table 4. Comparison of experimental and predicted values of Sh_{comp} and K_p

Re	Sh_{exp}/Sh_{pred} T	Sh_{exp}/Sh_{pred} D	$(K_p)_{exp}/(K_p)_{pred}$ T	$(K_p)_{exp}/(K_p)_{pred}$ D
1350	1.01	1.03	0.74	1.13
	0.96	1.03	0.83	1.21
2850	1.03	1.05	0.79	1.11
	0.97	1.04	0.92	1.21
5750	1.07	1.07	0.84	1.10
	1.00	1.06	1.00	1.20

Inspection of Table 3 indicates that, relative to the experimental data, the Delaware method predicts the variation of Sh_{comp} with L/D very well, while the Tinker method moderately overpredicts the variation. Similarly, for K_p, the Delaware method provides a better prediction of the variation with L/D, but both methods appear to underpredict the extent of the variation.

Whereas Table 3 dealt with the variation of the results with L/D, Table 4 compares the predicted results with those of experiment at each L/D and Re. To this end, Table 4 conveys the ratios Sh_{exp}/Sh_{pred} and $(K_p)_{exp}/(K_p)_{pred}$. At each Reynolds number, there are two lines of entries in the table. The first line conveys results for $L/D = 0.385$, while the second line is for $L/D = 0.585$. As before, the headings T and D respectively denote the predictions of the Tinker and the Delaware methods. Both the Sh and K_p of Table 4 are compartment-based quantities.

From the table, it is seen that for Sh_{comp}, both of the design methods predict the experimental results with acceptable accuracy, with the maximum deviation being 7%. The Delaware-method predictions are consistently low, whereas those of the Tinker method are either high or low depending on L/D. Overall, the Tinker predictions are somewhat closer to the experimental results.

The K_p values from the design methods show larger deviations from the experimental data than was the case for Sh_{comp}. In general, the K_p from the Tinker method are high while those from the Delaware method are low. Furthermore, whereas the Delaware predictions are closer to the data for $L/D = 0.385$, the Tinker predictions are closer for $L/D = 0.585$. Therefore, for the prediction of K_p, it would appear best to use the Delaware method at smaller interbaffle spacings and the Tinker method for larger interbaffle spacings.

Flow visualization

Photographs of the flow visualization patterns on the shell wall, on the surface of the baffle plate, and at each of the 49 unique tube positions are available

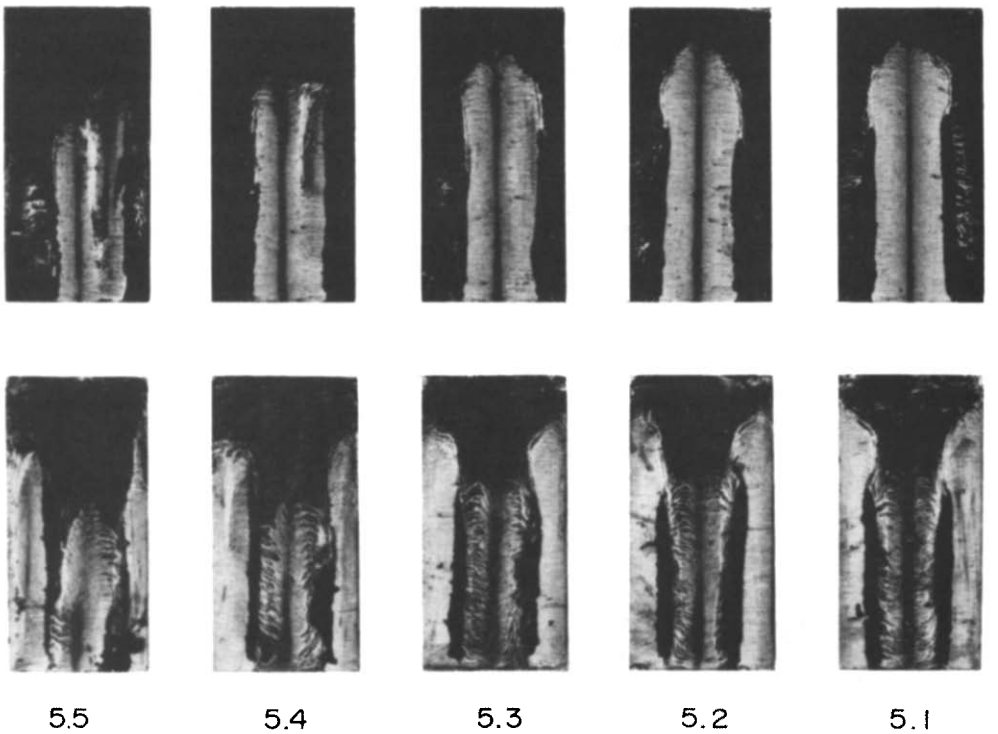

FIG. 9. Flow visualization patterns at the tubes of row 5 for $L/D = 0.385$.

in ref. [10]. Here, owing to journal space limitations, only a sample of the available information will be presented, and Fig. 9 has been prepared in this regard. As seen by the labels affixed to the figure, the visualization patterns pertain to the five unique tube positions in row 5, namely, positions 5,1 to 5,5.

Figure 9 consists of two tiers of photographs, with five photographs in each tier. The upper tier shows what is seen by an observer who stands upstream of the tubes and looks downstream. On the other hand, the lower tier is the view seen by an observer situated downstream of the tubes who looks upstream. The reason for obtaining the two views for each tube is to highlight the respective fluid flow patterns on the forward-facing and rearward-facing portions of the tube. To achieve definitive visualization patterns for each portion, it was necessary to use oil–lampblack mixtures of different fluidities (a more fluid mixture for the rear portion).

Each of the 10 photographs shown in Fig. 9 is a picture of the contact paper which had been affixed to the tube during the visualization run and had been removed and laid flat after the run. Prior to the run, the surface of the contact paper had been uniformly coated with the oil–lampblack mixture (and was, therefore, uniformly black).

Each of the upper-tier visualization patterns displays several common features. The narrow vertical line in the center of each pattern depicts the forward stagnation line. Emanating from the stagnation line is an array of very fine horizontal streaks embedded in a white background. These streaks represent a circumferential flow around the forward portion of the tube. The streaks terminate in a black region which reflects the separation of the flow from the surface of the tube. There is also a black region at the upper end of each visualization pattern. This black region is indicative of a pocket of separated flow which exists because the fluid which passes from one compartment to the next cannot execute a sharp turn. Note that the size of this pocket of separated flow increases in the direction from the symmetry line (BB′ in Fig. 2) toward the shell wall. Note also that at the shell-adjacent tubes 5,4 and 5,5, there are extra stagnation lines. These extra lines result because the fluid is moving outward toward the shell in order to fill the widening cross-sectional area.

The lower tier of photographs of Fig. 9 reveals the presence of a rear stagnation line. The stagnation line is flanked by a pair of counter-rotating eddies. In turn, the eddies are flanked by dark vertical bands which correspond to very slow-moving, separated fluid. The light-colored vertical bands at the edges of the photograph are the zone of circumferential flow mentioned in the preceding paragraph. Also in evidence in the upper reaches of these photographs is the black region which represents the pocket of separated flow associated with the turning of the fluid from one compartment into the next.

Flow visualization patterns for the heat exchanger of ref. [1] are presented in ref. [11]. A comparison of those results with the present visualization patterns confirms the expected channeling of the flow in the crossflow zone associated with the smaller interbaffle spacing.

CONCLUDING REMARKS

In the experiments described here, the response of the mass (heat) transfer and pressure drop on the shell side of a shell-and-tube heat exchanger to changes in the interbaffle spacing has been investigated. By means of the naphthalene sublimation technique, Sherwood numbers (dimensionless mass transfer coefficients) were determined at each tube in a typical compartment of the heat exchanger—a compartment situated in the region of hydrodynamically developed flow. The per-tube Sherwood numbers were used to evaluate row-average and compartment-average values. Sherwood numbers were also evaluated for a module consisting of two consecutive compartments.

Pressure distributions throughout the heat exchanger were also obtained, yielding not only the per-compartment pressure drop but also the pressure variation within a compartment. Flow visualizations were performed using the oil–lampblack technique. To supplement the experimental results, compartment Sherwood numbers and pressure drops were computed by applying the design methods of Tinker and of the Delaware Project.

The greatest sensitivity of the per-tube Sherwood numbers to the interbaffle spacing occurred at the tubes situated in the inflow window of the compartment. There, the greater the interbaffle spacing, the larger was the per-tube Sherwood number; the spacing-related effects were in the 15% range. In the crossflow zone, the per-tube Sherwood numbers corresponding to the smaller interbaffle spacing exceeded those corresponding to the larger interbaffle spacing by about 5%, and this relationship carried over into the baffle-adjacent row of tubes in the outflow window of the compartment. The other rows of tubes in the outflow window were ambivalent to the effect of the interbaffle spacing.

Despite the aforementioned per-tube responses to the interbaffle spacing, the compartment-average Sherwood numbers were virtually unaffected by the spacing.

The measured pressure distributions showed that within a given compartment, the pressure drop between the inflow end and the center of the compartment is substantially greater than the pressure drop between the center and the outflow end. The hydrodynamic development of the flow, as evidenced by the pressure distributions, was completed within the first compartment of the heat exchanger.

The per-compartment pressure drop decreased as the interbaffle spacing decreased. However, for the same streamwise length of heat exchanger, the pressure drop for the smaller interbaffle spacing slightly

exceeded (by about 6%) that for the larger interbaffle spacing.

Both the Tinker and the Delaware Project design methods yielded compartment Sherwood numbers which agreed satisfactorily with the experimental data. For the compartment pressure drop, the Delaware-based predictions are closer to the data at the smaller interbaffle spacing, while the Tinker-based predictions agreed better with the data at the larger interbaffle spacing.

REFERENCES

1. E. M. Sparrow and J. A. Perez, Internal, shellside heat transfer and pressure drop characteristics for a shell and tube heat exchanger, *J. Heat Transfer* **107,** 345–353 (1985).
2. T. Tinker, Shell side characteristics of shell and tube heat exchangers. In *General Discussion of Heat Transfer*, *Proc. Inst. Mech. Engrs*, London, pp. 89–116 (1951).
3. T. Tinker, Tube heat exchangers, a simplified rating system for commercial heat exchangers, *Trans. Am. Soc. mech. Engrs* **80,** 36–52 (1958).
4. K. J. Bell, Final report of the cooperative program on shell and tube heat exchangers, University of Delaware Engineering Experiment Station, Bulletin No. 5, Newark, DE (1963).
5. E. U. Schlünder (editor), *Heat Exchanger Design Handbook*, Vol. 3. Hemisphere, Washington, DC (1983).
6. W. Merzkirch, *Flow Visualization*. Academic Press, New York (1974).
7. H. H. Sogin, Sublimation from disks to air streams flowing normal to their surfaces, *Trans. Am. Soc. mech. Engrs* **80,** 61–71 (1958).
8. J. A. Perez and E. M. Sparrow, Determination of shellside heat transfer coefficients by the naphthalene sublimation technique, *Heat Transfer Engng* **6**(2), 19–30 (1985).
9. S. Whitaker, Forced convection heat transfer correlations for flow in pipes, past flat plates, single cylinders, single spheres, and for flow in packed beds and tube bundles, *A.I.Ch.E. Jl* **18,** 361–371 (1972).
10. L. G. Reifschneider, Effect of interbaffle spacing on the heat transfer and pressure drop in a shell and tube heat exchanger. Thesis, Department of Mechanical Engineering, University of Minnesota, Minneapolis, MN (1984).
11. J. A. Perez and E. M. Sparrow, Patterns of fluid flow in a shell-and-tube heat exchanger, *Heat Transfer Engng* **5**(3–4), 56–69 (1984).

EFFET DE L'ESPACEMENT DES BAFFLES SUR LE TRANSFERT THERMIQUE ET LA PERTE DE CHARGE DANS UN ECHANGEUR DE CHALEUR TUBE-CALANDRE

Résumé—Des expériences sont faites pour déterminer l'effet du changement de l'espace entre baffles sur le transfert de chaleur (masse) et la perte de charge côté calandre d'un échangeur. Des coefficients de transfert de chaleur (massse) par tube, par rangée et par compartiment sont obtenus à l'aide de la technique de sublimation du naphtalène, pour le régime pleinement établi. Des mesures de distribution de pression sont effectuées et la configuration de l'écoulement est visualisée à l'aide de la technique de la fumée d'huile. La plus grande sensibilité à l'espacement des baffles concerne les tubes situés dans la fenêtre d'entrée d'un compartiment, où les plus grands coefficients sont obtenus pour des grands espacements des baffles. Dans la zone d'écoulement transversal, les coefficients de transfert par tube pour le plus petit espacement des baffles sont supérieurs (5% environ) à ceux pour le plus grand espacement, et de façon semblable dans la région de la fenêtre de sortie du compartiment. Etant donné des compensations par zone, les coefficients de transfert moyens par compartiment sont virtuellement insensibles à l'espacement. La perte de charge par compartiment diminue quand l'espacement entre baffles décroît, mais pour une longueur fixée, la perte de charge est légèrement plus forte pour des espacements petits. Les résultats expérimentaux sont comparés aux prévisions des méthodes de conception Tinker et Delaware.

EINFLUSS DES SCHIKANENABSTANDS AUF DEN WÄRMEÜBERGANG UND DEN DRUCKVERLUST IN EINEM ROHRBÜNDEL-WÄRMEAUSTAUSCHER

Zusammenfassung—Es wurden Experimente durchgeführt, um die Auswirkungen des Schikanenabstands auf den Wärmeübergang und den Druckverlust im Mantelraum eines Rohrbündel-Wärmeaustauschers zu untersuchen. Die Wärmeübergangskoeffizienten pro Rohr, pro Rohrreihe und pro Schikanenteilung wurden mit Hilfe der Naphthalin-Sublimations-Methode ermittelt. Druckverteilungsmessungen wurden entlang des Wärmeaustauschers durchgeführt und die sich ausbildenden Strömungsbilder mit Hilfe der Öl-Flammruß-Methode sichtbar gemacht. Die größten Auswirkungen des Schikanenabstands auf den Wärmeübergang eines Rohres wurden bei Rohren festgestellt, die im Einströmfenster einer Teilung lagen, wobei höhere Übergangskoeffizienten (um etwa 15%) bei größeren Schikanenabständen auftraten. Im Kreuzstrom-Bereich sind die Wärmeübergangskoeffizienten bei geringeren Schikanenabständen um ungefähr 5% größer als bei größeren Abständen. Ähnlich verhält sich die Rohrreihe in Schikanennähe im Ausströmfenster der Teilung. Aufgrund der kompensierenden Wirkung der vorher erwähnten Erscheinungen für ein Rohr bleiben die Übergangskoeffizienten scheinbar unbeeinflußt vom Schikanenabstand. Der Druckabfall pro Teilung nahm nit abnehmendem Schikanenabstand ab, für eine bestimmte durchströmte Länge war jedoch der Druckverlust bei geringeren Abständen geringfügig größer. Die experimentellen Ergebnisse wurden mit den Aussagen nach dem Verfahren von Tinker und Delaware verglichen.

ВЛИЯНИЕ РАССТОЯНИЯ МЕЖДУ ПЕРЕГОРОДКАМИ НА ТЕПЛООБМЕН И ПЕРЕПАД ДАВЛЕНИЯ В КОЖУХОТРУБНОМ ТЕПЛООБМЕННИКЕ

Аннотация—Проведены эксперименты по определению влияния расстояния между перегородками на тепло(массо)обмен и перепад давления в кожухотрубном теплообменнике. Коэффициенты теплоотдачи отдельных труб, рядов труб и камеры при полностью развитом режиме получены методом сублимации нафталина. Распределение давления измерялось по всему теплообменнику; картина течения жидкости визуализировалась с помощью закопченого стекла. Наиболее сильная зависимость коэффициента теплоотдачи отдельной трубы от расстояния между перегородками наблюдалась в трубах, расположенных во впускном окне камеры, где бóльшим расстояниям между перегородками соответствуют бóльшие (на 15%) значения коэффициента. В зоне поперечного течения коэффициенты теплоотдачи отдельной трубы, соответствующие меньшим расстояниям между перегородками, на 5% превышали значения коэффициентов, полученные для бóльших расстояний; аналогичная ситуация наблюдается в ряду, примыкающем к перегородке, в выходном окне камеры. Другие ряды в выходном окне прямопротивоположно зависят от расстояния между перегородками. Благодаря гашению вынужденных реакций отдельной трубы, расстояние практически не влияло на коэффициенты теплоотдачи, осредненные по объему камеры. Перепад давления отдельной камеры уменьшался вместе с уменьшением расстояния между перегородками, в то время как для фиксированной по направлению течения длины значение перепада давления было немного больше для меньших расстояний. Результаты экспериментов сравнивались с расчетами по методам Тинкера и Делавере Прожект.